REMOTE SENSING AND MULTIVARIATE ANALYSIS FOR ASSESSING THE IMPACT OF PLANT DIVERSITY ON LAND SURFACE TEMPERATURE OF WADI AL-SHARAEA, MAKKAH REGION, SAUDI ARABIA

EL-MORSY, M. H.[1] – ABD EL-HAMID, H. T.[2*] – OSMAN, H. E.[3] – ELAIDAROUS, A. A.[3]

[1]*Deanship of Postgraduate Studies and Research, Umm Al-Qura University, Makkah, Saudi Arabia*

[2]*National Institute of Oceanography and Fisheries, NIOF, Alexandria, Egypt*

[3]*Biology Department, Faculty of Science, Umm-Al-Qura University, Makkah, Saudi Arabia*

**Corresponding author*
e-mail: ht.abdelhamid@niof.sci.eg

(Received 3rd Dec 2023; accepted 19th Apr 2024)

Abstract. Nowadays, studying the macrophytes distribution climatic change reducing effect through land surface temperature is vital. 17 locations with 102 stands were randomly chosen to illustrate the vegetation physiognomy in Wadi Al-Sharaea, Makkah Province, Saudi Arabia. A total of 110 species from 77 genera and 33 families were detected during the field study, with the Poaceae family predominant. Therophytes were the dominant life form (38.2% of the total species), followed by chamaephytes (30.0%), and bioregional elements were the dominant chorotype. Remote sensing data were acquired to evaluate land surface temperature (LST), normalized difference built-up index (NDBI), and normalized difference vegetation index (NDVI) from 2002 and 2018. The study assesses the relationship between organic matter, plant diversity species, vegetation cover, and LST. Principal component analysis (PCA) was applied, and the obtained data showed that PCA1 and PCA2 represent about 25.29% and 16.34%, respectively. Cluster analysis was used to identify the commonality of the groups among the data from points clustered into four significant clusters. On the other hand, LST correlated with the distribution of some families, such as Caryophyllaceae, Boraginaceae, Euphorbiaceae, and Molluginaceae. The families that correlated to LST show the tolerance of these families to high temperatures. Results showed that *Limeaceae, Poaceae,* and Zygophyllaceae families grow in soil with high organic matter**.** These findings indicated fundamental advances in understanding the temperature response of organic matter and plant diversity.
Keywords: *vegetation, normalized difference built-up index (NDBI), normalized difference vegetation index (NDVI), PCA, cluster analysis*

Introduction

Over the last century, global temperature has risen by 0.5°C (Folland et al., 1990). Temperature increases are anticipated to persist and intensify with the ongoing increase in greenhouse gases in the environment. It is uncertain if this will result in a decrease or gain in soil organic C. If it results in a drop in soil organic carbon, that carbon would need to be converted to carbon dioxide (CO_2), increasing the current quantity in the atmosphere and positively impacting climate change. Soil organic matter (SOM) is usually produced by vegetation activity in the soil and is an important index of soil fertility (Tadini et al., 2021). One of the most crucial elements of climate change research is the measurement of LU/LC variations at the local scale. LST is the most significant environmental factor used to estimate the exchange of energy and matter between the Earth's surface and the lower atmosphere (Feddema et al., 2005). Changes

http://www.aloki.hu ● ISSN 1589 1623 (Print) ● ISSN 1785 0037 (Online)
DOI: http://dx.doi.org/10.15666/aeer/2203_25672587

in LULC have been demonstrated to substantially impact the climate through several mechanisms that affect LST and precipitation (Joshi et al., 2020). Analyzing trends at various time scales is made possible by remotely sensed data. Technology advancements have made it possible to collect optical and thermal data from the same sensor platforms, which is useful for analyzing thermal conditions and changes in urban land cover (Choe and Yom, 2020). Because plant cover is a significant component of the terrestrial ecosystem, vegetation has a direct or indirect relationship to the energy cycle, hydrology, soil, and climate (Chandra et al., 2023). Following the industrial revolution, global warming raised the LST. The characteristics of human activity, changes in the terrestrial ecosystem, soil ecosystems, hydrology, and the process of regional and global climate change are all significantly influenced by the amount of vegetation cover (Islam et al., 2021). Moderate-resolution sensors like Landsat, ASTER, and MODIS are frequently used to evaluate how land use and land cover changes affect the thermal environment (Zhang et al., 2021). To gain the synoptic picture needed to comprehend the interaction between natural processes and human modification of those processes, remote sensing data must be incorporated into the study of urban climate. One of the vegetation indicators frequently used to assess plant greenness is the normalized difference vegetation index (NDVI) (Mondino et al., 2016). The normalised difference built-up index (NDBI) change can also be used to detect changes in LULC. This index provides information about the built-up area, especially in urbanized areas (Ibrahim, 2017). The reverse of NDVI is NDBI. Whereas NDVI denotes land covered in greenery or plants, including vegetation, agricultural land, parks, gardens, and open space, NDBI indicates the built-up area (impervious area), including bare land. It is possible to anticipate that there will be a negative association between NDVI and NDBI. The second goal of this study will likewise cover this issue. The current work objectives can be summed up as follows: 1) To examine the link between LST from Landsat imageries data among NDVI, NDBI; 2) to evaluate the families that bear high temperature in relation to organic matter of the soil.

Materials and methods

Study area

This study was conducted in Wadi Al-Sharaea, Makkah region in the western region of Saudi Arabia. All measurements, plants, and soil samples were taken from February 2018 to January 2021. Plant and soil samples were taken at seventeen (17) sites for Wadi Al-Sharaea. A handheld Global Positioning System (GPS) was used to determine the study area’s geographical locations, and the maps of all locations were drawn by ArcGIS version 10.8. The study area is Wadi Al Sharara, located southeast of Makkah Al Mukarramah city, and it is one of the main sub-basins of Wadi Auranah, which flows towards the central region of Makkah Al Mukarramah. The total area of the valley is 638.98 km², and it receives water mainly from the drained groundwater. The basin is located astronomically between geographic coordinates 21°36`01” N to 21°19`28”N and 39°16`21” to 40°55`40”E (*Fig. 1*; *Table 1*). During field survey, some photos of plant species were taken as shown in *Figure 2*.

http://www.aloki.hu ● ISSN 1589 1623 (Print) ● ISSN 1785 0037 (Online)
DOI: http://dx.doi.org/10.15666/aeer/2203_25672587

Climate

Saudi Arabia's climate is remarkably diverse; weather conditions are typically consistent since most of the nation is a desert-like plateau. Summers in most of the country are dry and hot; however, winters are mild, with temperatures falling at night and rain to be anticipated. Precipitation is uncommon but may be substantial during the winter months of December to February (*Table 2*).

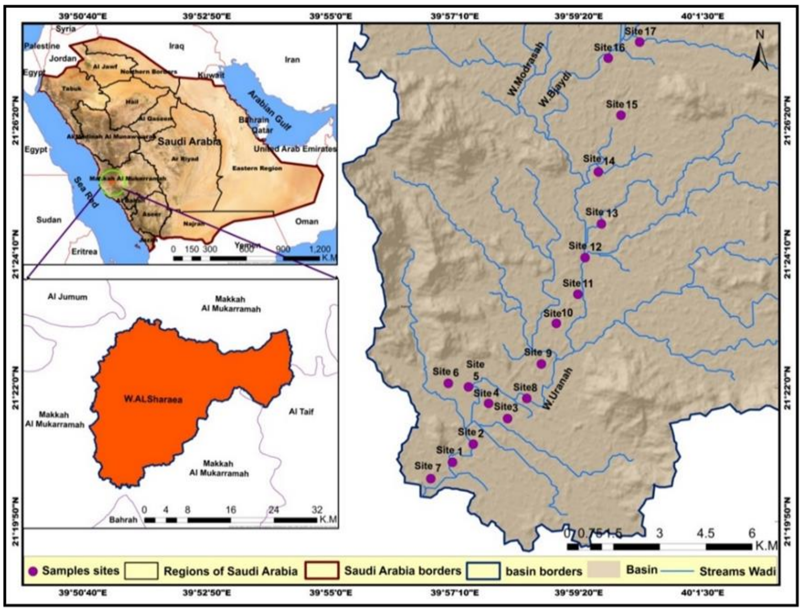

***Figure 1.** Maps of study area of Wadi Al-Sharaea, Makkah Province, Saudi Arabia*

***Figure 2.** Photos of plants as shown from left to right respectively; (1) Malva parviflora, (2) Corchorus depressus, (3) Sisymbrium irio, (4) Euploca strigosa*

http://www.aloki.hu ● ISSN 1589 1623 (Print) ● ISSN 1785 0037 (Online)
DOI: http://dx.doi.org/10.15666/aeer/2203_25672587

Table 1. *Study site locations (latitude and longitude along Wadi Al-Sharaea, Makkah Province, Saudi Arabia*

Site ID	Latitude (DD MM SS)	Longitude (DD MM SS)
1	21° 20’ 47.7”	39° 57’ 07.6”
2	21° 21’ 05.3”	39° 57’ 29.4”
3	21° 21’ 30.2”	39° 58’ 05.3”
4	21° 21’ 45.0”	39° 57’ 45.4”
5	21° 22’ 01.0”	39° 57’ 24.3”
6	21° 22’ 04.5”	39° 57’ 03.2”
7	21° 20’ 31.8”	39° 56’ 44.8”
8	21° 21’ 49.8”	39° 58’ 25.5”
9	21° 22’ 23.3”	39° 58’ 40.8”
10	21° 23’ 02.8”	39° 58’ 56.5”
11	21° 23’ 31.1”	39° 59’ 19.1”
12	21° 24’ 06.7”	39° 59’ 26.6”
13	21° 24’ 39.5”	39° 59’ 43.7”
14	21° 25’ 30.1”	39° 59’ 40.5”
15	21° 26’ 25.1”	40° 0’ 04.2”
16	21° 27’ 20.6”	39° 59’ 50.9”
17	21° 27’ 36.3”	40° 0’ 23.8”

Table 2. *Data on climate along the study area*

Month	Temperature (°C) mean			Humidity (%)			Wind (knots/h)	Rainfall (mm) monthly	Humidity (%)		
	MX	MN	M	MX	MN	M			MX	MN	M
1	31.3	18.3	24.8	97	15	56	3	0.0	97	15	56
2	33.1	19.6	26.4	96	16	53	4	0.5	96	16	53
3	35.5	20.8	28.2	85	10	43	4	0.0	85	10	43
4	38.3	24.1	31.2	89	7	41	4	4.0	89	7	41
5	42.5	27.4	35.0	79	7	34	4	23.6	79	7	34
6	44.2	29.8	37.0	83	8	30	4	18.7	83	8	30
7	43.3	29.3	36.3	82	9	29	3	0.0	82	9	29
8	42.4	28.9	35.7	97	11	38	4	36.2	97	11	38
9	42.5	28.3	35.4	95	9	47	4	27.1	95	9	47
10	38.8	25.3	32.1	92	10	53	3	57.2	92	10	53
11	33.9	22.5	28.2	96	21	61	3	45.0	96	21	61
12	31.5	20.5	25.3	97	19	60	3	7.5	97	19	60
MX	44.2			97				219.4	97		
MN		18.3			7					7	
M			30.9			45	4	18.3			45

Vegetation data collection

Along Wadi Al-Sharaea’s studied region, seventeen sites (location) were chosen. The main canal of Wadi Al-Sharaea, Makkah Al-Mukarramah, was randomly selected as the representative location, and six quadrats (5 m X 5 m) were used for each area to

http://www.aloki.hu ● ISSN 1589 1623 (Print) ● ISSN 1785 0037 (Online)
DOI: http://dx.doi.org/10.15666/aeer/2203_25672587

measure and classify the growing plants. Density, relative density, frequency, relative frequency, cover, and relative cover were estimated according to Mueller-Dombois & Ellenberg (1974). Also, according to Ludwing and Reynolds (1988), the significance value (IV) could be calculated by summing the relative density, frequency, and cover for each family under investigation. Plant samples were kept as herbarium sheets after being pressed and dried for checking and identification, then named according to Chaudhary (1989), Migahid (1996), and Collenette (1999). The names of most plants and their families have been updated according to the websites of the following flora : Plants of the World Online (POW, http://www.plantsoftheworldonline.org/),Catalogue of Life (COL, https://www.catalogueoflife.org/) and Flora of Saudi Arabia Checklist (FOSAC, http://plantdiversityofsaudiarabia.info/Biodiversity- Saudirabia/Flora /Checklist/Cheklist.htm.

Data source and image pre-processing

The study employed satellite images from 26-7-2002 and 17-4-2018 from the Landsat 5 Thematic Mapper (TM) and Landsat 8- Operational Land Imager (OLI). Images from the US Geological Survey's (USGS) Landsat satellite; https://earthexplorer.usgs.gov. The entire study area, including Path 170 and Row 45. ENVI 5.3 software was used to perform radiometric corrections and image enhancement operations prior to analysis (Abd El- Hamid et al., 2020).

Land use and land cover (LULC) classification

Land use and land cover (LULC) classification automatically categorize each image's cells into various land cover classifications. Previous studies have classified satellite imagery cells into several LULC classes using multi-temporal Landsat satellite imagery using various classification techniques (Rimal et al., 2017). LULC in the present study was applied according to the Sentinel-2 10 m Land Use/Land Cover website.

Calculation of vegetation cover

By measuring the difference between the electromagnetic spectrum's near-infrared and red portions, NDVI quantifies the amount of vegetation present (Malik et al., 2019). Visible light is absorbed by dense, healthy vegetation, but the majority of near-infrared light is reflected. On the other hand, poor vegetation reflects less near-infrared light and more visible light. The NDVI scales from +1 to -1, with +1 denoting good vegetation and -1 denoting bare ground. As indicated in the equation below, NDVI was estimated in ArcGIS 10.7 using the NIR Band 5 and Red Band 4 of Landsat-8 and the NIR Band 4 and RED Band 3 of Landsat-5 data (Rogan et al., 2013; Kikon et al., 2016).

$$\mathrm{NDVI} = \frac{Near - Red}{Near + Red} \tag{Eq.1}$$

Calculation of normalized difference built-up index (NDBI)

Built-up is distinguished from other land uses and land surfaces by the NDBI, which varies from -1 to + 1. Built-up areas reflect more light in MIR than NIR. Therefore, the built-up areas are indicated by the high NDBI values. As stated in the equation, The MIR Band 6 and NIR Band 5 of Landsat-8 and the MIR Band 5 and NIR Band 4 of Landsat-5 data were used to calculate NDBI in ArcGIS 10.6 (Zha et al., 2005).

http://www.aloki.hu ● ISSN 1589 1623 (Print) ● ISSN 1785 0037 (Online)
DOI: http://dx.doi.org/10.15666/aeer/2203_25672587

$$\text{NDBI} = \frac{MIR - NIR}{MIR + NIR} \quad \text{(Eq.2)}$$

Land surface temperature (LST)

Grasp the economic flow of energy between the Earth's surface and the local environment requires a thorough grasp of surface temperature. The surface temperatures were computed using the sensors' radiance values. The surface temperatures were extracted using the procedures listed below.

Digital number (DN) conversion to radiance

The temperature bands used to estimate LST for operational land imager (OLI) and Thematic Mapper ™ were bands 10 and 6, respectively. As indicated in the following equation, QGIS was used to convert digital number (DN) to radiance (Barsi et al., 2014):

$$L\lambda = ML * Q\text{cal} + AL - Oi \quad \text{(Eq.3)}$$

where AL is the band-specific additive rescaling factor; ML is the band-specific multiplicative rescaling factor; Q_{cal} is the image of band 10; O_i is the correction of band 10.

Maximum conversion of light to temperature

The band data should be skillfully translated to brightness temperature (BT) using the thermal constants given in the metadata file once DN has been transformed to radiances. The following formula is used to convert using the equation:

$$TB = \frac{k_1}{In\left[\left(\frac{k_1}{L_\lambda}\right)\right] + 1} - 273.15 \quad \text{(Eq.4)}$$

where K_1 represents a band-specific thermal conversion derived from metadata and K_2 represents a band-specific thermal conversion derived from metadata; BT: Satellite brightness temperature (Celsius); The assumption made by brightness temperatures that the globe is a blackbody, which is incorrect, can quickly lead to inaccuracies in surface temperature. To eventually acquire the LST from BT, emissivity correction must be performed because it helps to minimize these mistakes.

NDVI's land surface emissivity (LSE)

Three formulae were provided to determine the ground surface's emissivity. The efficiency of thermal energy flow across the surface and into the atmosphere, as depicted in the equation. Blackbody radiance (Planck's law) is scaled using the LSE proportionality factor to forecast emitted radiance. LSE is a proportionality coefficient that modifies the black body's brightness (according to Planck's law) to forecast the radiation that is emitted (Sobrino et al., 1990).

$$\varepsilon_\lambda = \varepsilon_V P_V + \varepsilon_\lambda (1 - P_V) + d\varepsilon \quad \text{(Eq.5)}$$

$$d\varepsilon = (1 - \varepsilon s)(1 - Pv) F \varepsilon v \quad \text{(Eq.6)}$$

$$P_V = (\text{NDVI}_{max} - \text{NDVI}_{min}) / \text{NDVI}_{max} + \text{NDVI}_{min}) \quad \text{(Eq.7)}$$

http://www.aloki.hu ● ISSN 1589 1623 (Print) ● ISSN 1785 0037 (Online)
DOI: http://dx.doi.org/10.15666/aeer/2203_25672587

$$\text{NDVI} = \frac{OLI\ band\ 5 - TM\ band\ 4}{OLI\ band\ 5 + TM\ band\ 4} \qquad \text{(Eq.8)}$$

where Pv is the vegetation proportion, v is the emissivity of vegetation, s is the soil emissivity, and F is a shape factor with a mean value of 0.55 under various geometrical distributions. Assuming different geometric distributions, where v is vegetation emissivity, Pv is vegetation’s proportion, s is soil’s emissivity, and F is the form factor with an average value of 0.55.

Land surface emissivity (LST °C) calculation

The LST can be ascertained using the subsequent equation after the emissivity image have been acquired:

$$\text{LST} = \frac{BT}{1 + \frac{\lambda(BT) * \ln \varepsilon}{\rho}} \qquad \text{(Eq.9)}$$

where the sensor brightness temperature (BT) is indicated in Celsius (°C). Celsius (°C) is used to express LST. The wavelength of the radiation that is emitted is λ (11.5 μm). ρ is the Stefan–Boltzmann constant, ε is the land surface emissivity, c is the light velocity, h is Planck’s constant, and (LSE) = h * c/σ = $1.438 * 10^{-2}$ mK.

Statistical analysis

The principal component analysis (PCA) was used to guarantee that the data’s dimensionality was reduced, and that the PCs’ combinations of factors most significantly affected sample variability. The principal components (PCA) is the most widely used technique for measuring and condensing a group of related variables into a smaller set of variables. Cluster analysis was used to highlight the similarity of data along the study region, in contrast to principal component regression, which seeks hyperplanes of maximum variance among the independent variables and response. Multivariate techniques that group items according to their attributes are referred to as cluster analysis. Clustering things makes them more similar to one another than the objects in other groups. By putting soil samples into groups based on similarities, Morrison et al. (2011) successfully classified soil samples using cluster analysis.

Results and discussion

Plant diversity

The findings indicated that 110 species of plants belonging to 77 genera and 33 plant families, as shown in (*Tables A1* and *A2*). The most dominant family is Poaceae family (21 species), followed by Fabaceae (13), Boraginaceae (8), Asteraceae (7), and Zygophyllaceae (6). Furthermore, the rest of the families have fewer than six species for each, and one exclusively represented 15 families (Araceae, Asphodellaceae, Capparaceae, Euphorbiaceae, Gisekiaceae, lamiaceae, Limeaceae, Neuradacaeae, Orobanchaceae, polygonaceae, Portulacaceae, Rubiaceae, Rutaceae, Tamaricaceae and Urticaceae). Therophytes dominated the life forms of the recognized species (38.2% of the total species), followed by chamaephytes (30.0%). Hydrophytes were represented by one species (*Lemna gibba*) (0.9%). Furthermore, the surviving phytogeographical

http://www.aloki.hu ● ISSN 1589 1623 (Print) ● ISSN 1785 0037 (Online)
DOI: http://dx.doi.org/10.15666/aeer/2203_25672587

distribution indicated that bioregional taxa (43.6% of the total species) dominated the other chorotypes. These findings are congruent with those of Elaidarous et al. **(**2022**).**

Tribulus pentandrus- Stipagrostis plumosa community was significantly affected with silt, while the communities dominated by *Maerua crassifolia- Cynanchum radians* and *Rhazya stricta- Polycarpaea repens* were affected with coarse sand (Elaidarous et al., 2022).

Distribution of organic matter

Results showed a significant variation in organic matter concentrations along the study area. The concentration of organic matter ranged from 0.01 to 4.5 mg/kg as shown in *Table 3*. High concentration was observed in the southern part of the study area, whereas low and moderate concentrations were observed in the northern part of the study area. The productivity of soil depends on organic matter. Therefore, as shown from organic matter distribution, the southern part is more suitable for cultivation than the northern part. Remote sensing data showed a great relationship between LST and the moisture content of soil (Bonn and Neill, 1993). But recent studies reveal that it is possible to relate LST to soil attributes, such as texture (Osińka-Skotak, 2007; Wang et al., 2015) and organic matter (OM) content (Zhao et al., 2014). Due to their various thermal characteristics, sand, clay, and OM-varying soils can improve LST differentiation. According to Osika-Skotak's (2007) research, topsoil texture significantly influences LST and can cause variances in brightness temperatures of up to 4 °C for the same type of soil. Since soil's thermal qualities significantly impact LST, these variations are closely tied to the amount of water in the soil. LST's behavior in reaction to soil moisture so reveals details about the texture of the soil (Wang et al., 2012; Wang et al., 2015; Müller et al., 2016).

Table 3. *Mean soil chemical analysis of Wadi Al-Sharaea, Makkah Province, Saudi Arabia. (n = 6)*

Site	pH	EC	TDS	Ca	Mg	Na	K	CO_3	HCO_3	SO_4	Cl	OM
		dS/m	mg/l	meq/l								%
1	8.7	0.12	63.75	0.41	0.52	0.17	0.08	Nil	0.74	0.18	0.31	0.968
2	9.43	0.13	65.00	0.62	0.48	0.11	0.03	Nil	0.68	0.15	0.43	1.083
3	8.92	0.14	80.17	0.77	0.59	0.11	0.05	Nil	0.69	0.14	0.71	1.076
4	8.60	0.74	425.50	4.12	1.57	1.44	0.18	Nil	1.64	2.28	3.51	1.817
5	7.85	0.14	88.25	0.81	0.34	0.24	0.10	Nil	0.55	0.57	0.40	1.937
6	8.43	0.42	255.00	2.69	0.73	0.55	0.16	Nil	0.55	1.84	1.90	1.937
7	9.08	0.11	66.75	0.53	0.42	0.14	0.06	Nil	0.48	0.39	0.33	1.363
8	7.75	0.15	84.00	1.07	0.22	0.16	0.07	Nil	1.01	0.24	0.31	0.924
9	8.03	0.15	81.25	0.99	0.29	0.12	0.08	Nil	0.96	0.27	0.27	0.810
10	8.25	0.17	95.00	1.31	0.16	0.14	0.09	Nil	1.11	0.29	0.34	5.551
11	7.65	0.11	68.00	0.75	0.24	0.20	0.08	Nil	0.54	0.39	0.28	4.602
12	8.35	0.13	74.50	0.80	0.33	0.14	0.08	Nil	0.85	0.28	0.26	3.981
13	8.08	0.17	92.00	0.93	0.50	0.10	0.13	Nil	1.03	0.36	0.31	1.311
14	7.39	0.05	30.27	0.82	0.20	0.02	0.08	Nil	0.10	0.10	1.79	1.097
15	7.35	0.05	31.68	1.09	0.31	0.06	0.13	Nil	0.10	0.12	1.86	1.098
16	7.32	0.09	54.68	2.37	0.41	0.04	0.39	Nil	0.10	0.11	1.89	1.516
17	7.52	0.05	22.99	0.71	0.46	0.03	0.42	Nil	0.10	0.02	2.19	1.388

http://www.aloki.hu ● ISSN 1589 1623 (Print) ● ISSN 1785 0037 (Online)
DOI: http://dx.doi.org/10.15666/aeer/2203_25672587

Land use and land cover (LULC) classification

Six classes were applied in the present study, water bodies, trees, crops, built-up, bare lands, and rangelands as: 0.05499 km^2 (0.0109%), 1.2113 km^2 (0.24%), 44.1908 km^2 (8.7796%), 42.2498 km^2 (8.394%), 245.3467 km^2 (48.744%) and 170.2764 km^2 (33.8299%) respectively. It was shown that bare lands were the highest, whereas water bodies were the lowest compared to other classes, as shown in *Fig.3*. In general, the amount and kind of vegetation that reflects its usage, environment, cultivation, and seasonal phenology are used to categorize LULC and demonstrate the landscape's characteristics. Runoff and flash floods are also significantly influenced by land cover. The land surface temperature decreases as a land cover's biomass/vegetation abundance increases. Additionally, inland water and built-up areas had a higher mean value than vegetative land uses (Weng et al., 2004). The LST in vegetation is the lowest. Strong forest vegetation's ability to reduce the heat stored in the soil and surface structures through transpiration may help explain this outcome (Weng and Lu, 2008).

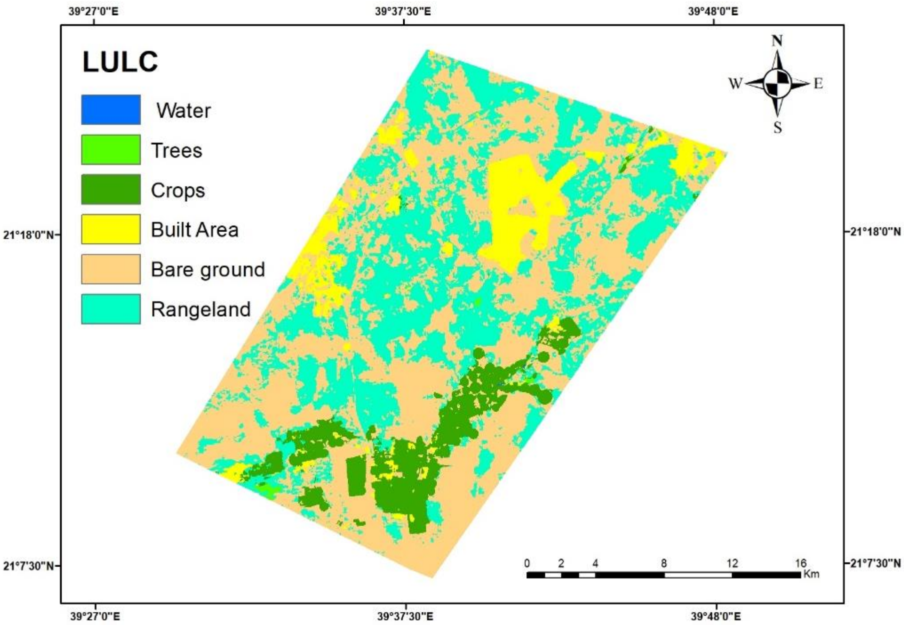

Figure 3. *LULC classification map of the study area*

Land surface temperature (LST) distribution

The increase in temperature was observed in bare and built-up lands. Data from satellite images confirm the field data of temperature. *Figure 4* displays LST maps from 2002 and 2018 for the study area. Similarly, LST values in metropolitan areas have also increased. The maximum and average temperatures in the research area have generally increased over the past 16 years. The findings of this study's land surface temperature (LST) analysis may help us comprehend temperature fluctuation in different locations. This will lessen the urban heat island effect, enabling planners to make sustainable plans. Temperature is less in the areas where dense vegetation is present. Also, vegetation cover is the cause the less thermal radiation.

http://www.aloki.hu ● ISSN 1589 1623 (Print) ● ISSN 1785 0037 (Online)
DOI: http://dx.doi.org/10.15666/aeer/2203_25672587

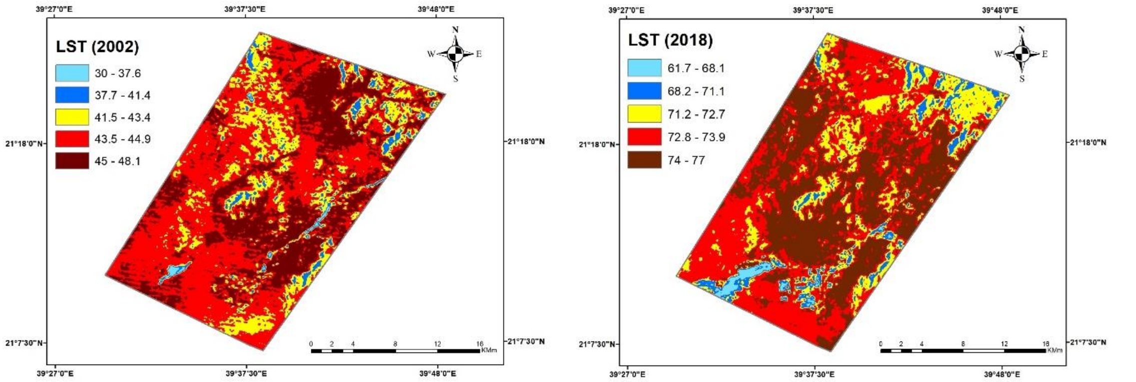

Figure 4. *LST maps for the years 2002 and 2018*

Normalized difference built-up index (NDBI) analysis

Numerous studies have used NDBI because it makes it easier to separate populated regions from other land uses and land cover (Chen et al., 2006). The NDBI density maps are given in *Fig.5*. According to Ranagalage et al. (2018), built-up areas have significantly higher positive NDBI values than bare lands, which have minor positive values. However, in several cases, the NDBI values indicating residential were different (Xu and Zhang, 2017). In this study, the NDBI value for the built-up areas in 2002 and 2018 was 0.2 and 0.3, respectively. The loss in vegetation and the growth of the residential regions, consistent with the findings of Maskooni et al. (2021), was the cause of the significant increase in NDBI value.

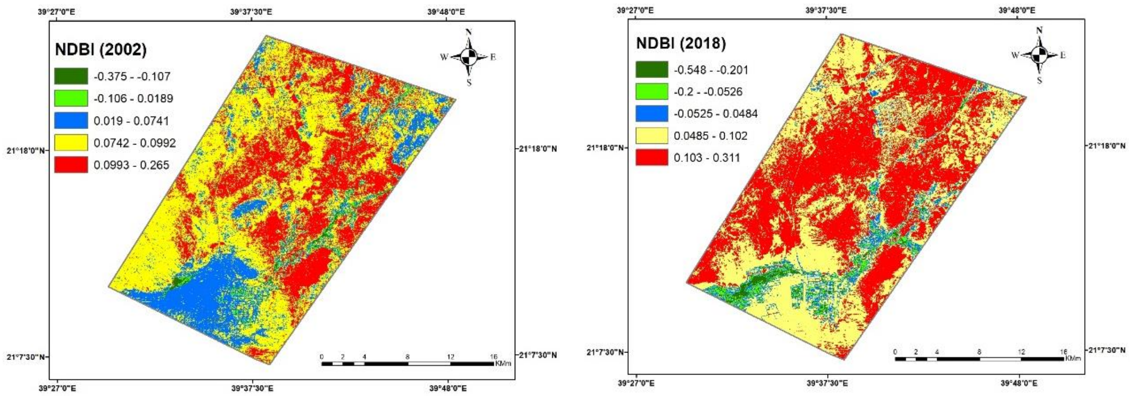

Figure 5. *NDBI density map in 2002 and 2018*

Normalised difference vegetation index (NDVI) analysis

The Normalised Difference Vegetation Index (NDVI) recognizes and monitors vegetation. Numerous research studies have examined the relationship between NDVI and urban heat islands (UHI). The correlation between LST and NDVI is shown in *Figure* 5. Results showed that there is a negative relationship between NDVI and LST. Similarly, other research found that as plant cover decreased, the land surface temperature rose (Maskooni et al., 2021). This study also looked at how variations in NDBI impacted NDVI results. As a result, it was discovered that NDBI and NDVI have

http://www.aloki.hu ● ISSN 1589 1623 (Print) ● ISSN 1785 0037 (Online)
DOI: http://dx.doi.org/10.15666/aeer/2203_25672587

a bad association. According to Roy et al. (2020), the expansion of urban areas caused previously green spaces to transform into built-up areas. These results are consistent with those of Kant et al. (2009), who found that places with bare soil and built-up regions have higher LST values during the daytime than other categories, including water bodies, agriculture, and vegetation. Built-up and arid environments, on the other hand, have lower LST values at night, while water bodies and vegetation are observed to have greater LST values. *Figure 6* shows an inverse relationship between LST and OM in the same vein as (Guha et al., 2018). This is acceptable because NDVI readings ranged from dense to weak vegetation and, in some cases, barren terrain. Greater NDVI values are produced by heavily vegetated areas in spatiotemporal analysis.

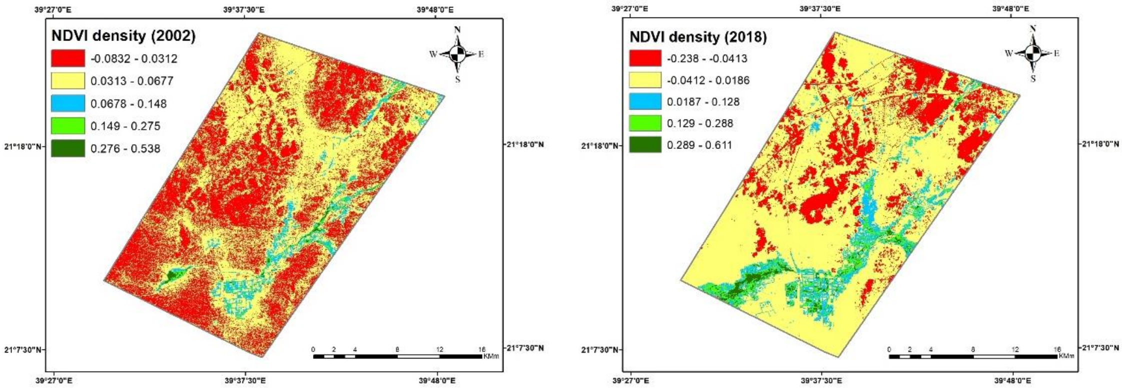

Figure 6. *NDVI density map of 2002 and 2018*

Principal component analysis (PCA) and cluster analysis

From PCA analysis, sites 10 and 13 have different characteristics than other sites. Data showed that components 1 and 2 represent about 25.29% and 16.34%, respectively, as shown in *Figure 7*; organic matter was correlated with Poaceae, Limeaceae, and Zygophyllaceae.

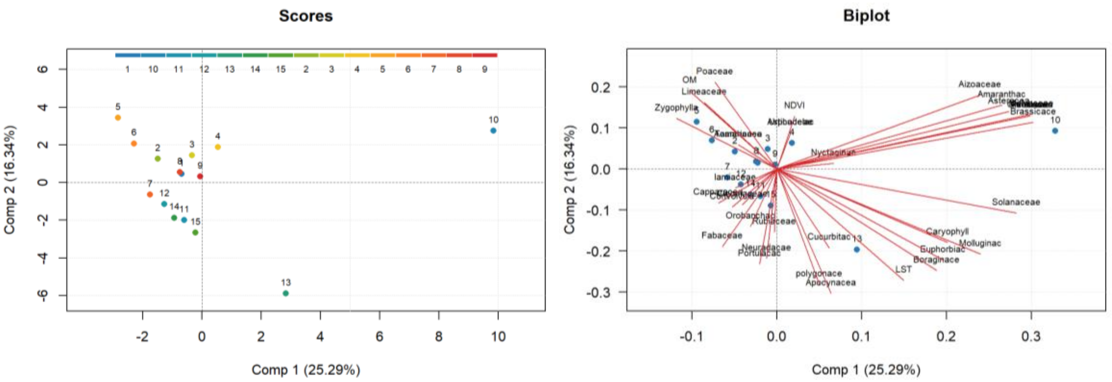

Figure 7. *PCA analysis of sampling sites and plant families among organic matter with LST along the study area*

Cluster analysis was used to identify the commonality of the groups among the data from points clustered into four significant clusters. On the other hand, LST was correlated with

http://www.aloki.hu ● ISSN 1589 1623 (Print) ● ISSN 1785 0037 (Online)
DOI: http://dx.doi.org/10.15666/aeer/2203_25672587

some families, such as Caryophyllaceae, Boraginaceae, Euphorbiaceae, and Molluginaceae, respectively. The families that correlated to LST show the bearing of these families to high temperatures. The date of the cluster analysis confirms the same data of PCA, and the families that correlated to LST show the same characteristics as shown in *Figure 8*. According to cluster analysis, Lamiaceae, Poaceae, and Zygophyllaceae families grow in soil with high organic matter.

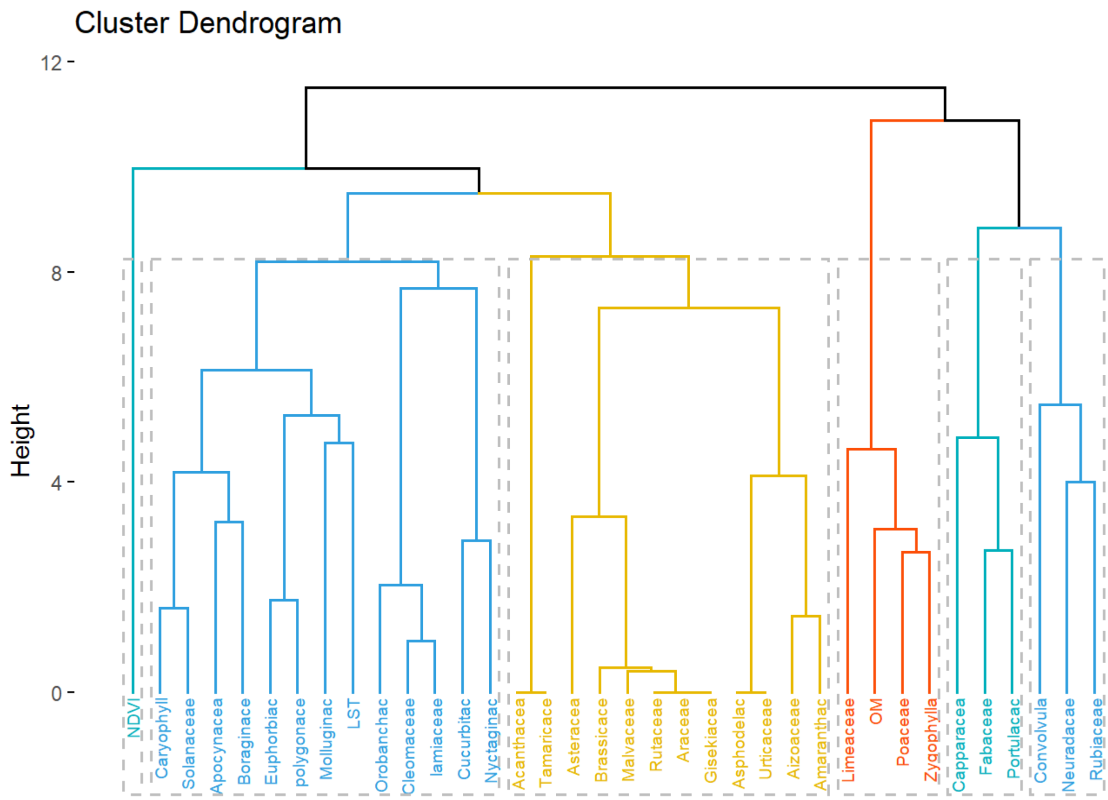

Figure 8. *Cluster analysis of plant families among organic matter and LST*

Regression model among LST with NDVI and OM

The produced regression model explains the relation with R 2 Te regression line produced a definitive explanation, showing a strong negative relationship among LST NDVI and organic matter as shown in *Figures 9* and *10*. For NDVI and LST relation, statistical linear regression analysis indicated that kappa coefficient values were $R^2 = 0.12$ and 0.26 with organic matter. Results showed that the soil's organic matter contributed to the decrease in LST as NDVI. Finally, NDVI values can be used to assess the effect of climate change on vegetation productivity in different periods (Rani et al., 2018). Variations in land use and cover, as well as direct and indirect effects of climate change on vegetation, can all be reflected in variations in NDVI and NDBI values. A satellite is an important tool for gathering information about an object from a distance. Extended analyses of the dynamics of RS vegetation have become increasingly important in studying global ecosystems (Hussain et al., 2023).

http://www.aloki.hu ● ISSN 1589 1623 (Print) ● ISSN 1785 0037 (Online)
DOI: http://dx.doi.org/10.15666/aeer/2203_25672587

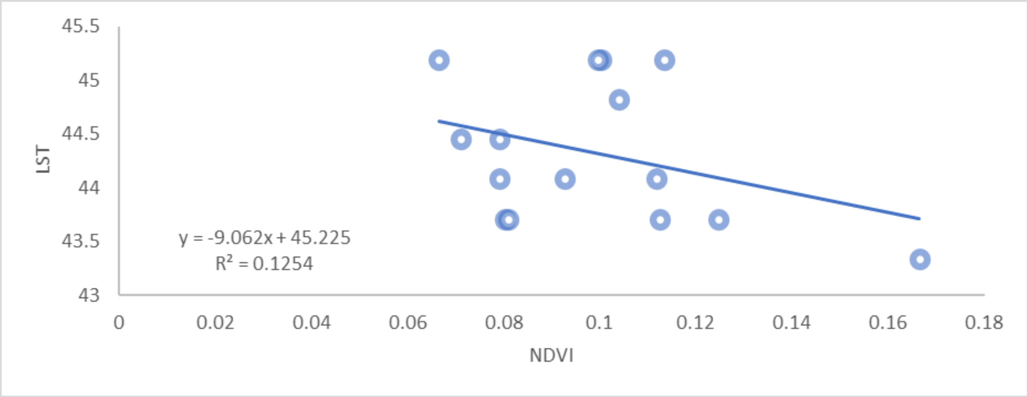

Figure 9. *Relationship between LST and NDVI*

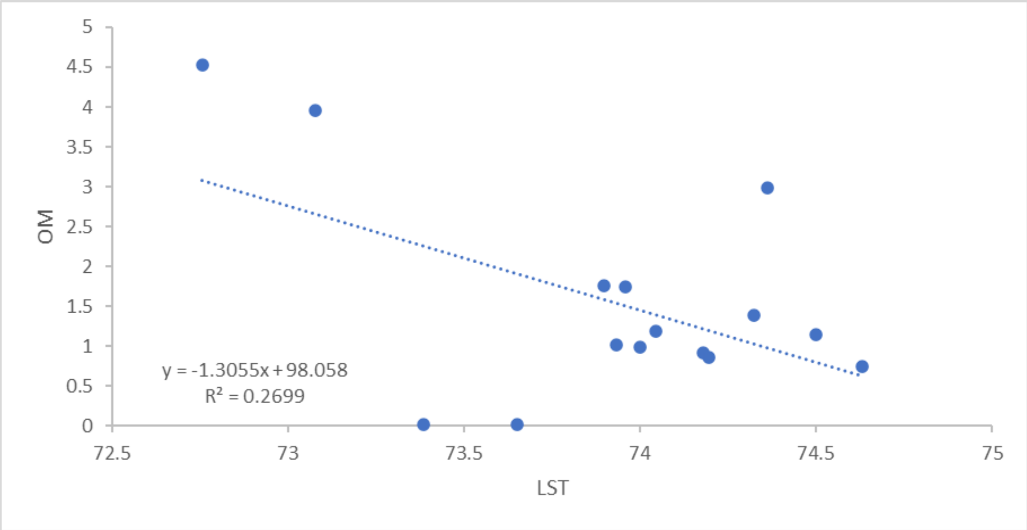

Figure 10. *Relationship between LST and OM*

Conclusion

To estimate the change in the LST in Wadi Al-Sharaea, Makkah, Saudi Arabia, over 16 years, LST data from 2002 and 2018 were compared in this study. According to the study's findings, the average temperature was 39°C in 2002 but increased to almost 45°C in 16 years. NDVI and NDBI were used to identify the spatial variations in the LST values. In order to describe LST relationships, NDVI and NDBI studies were carried out, and a linear regression analysis was produced. The study's findings indicated a negative correlation between LST and NDVI, suggesting that surfaces with vegetation had lower land surface temperatures. Built-up locations have greater LST values when compared to vegetated areas. It was found that there is a significant positive link between NDBI and LST, which explains why barren regions and metropolitan locations have higher temperatures. Data from organic matter showed a positive correlation with Poaceae, Limeaceae, and Zygophyllaceae.

On the other hand, LST was correlated with some families, such as Caryophyllaceae, Boraginaceae, Euphorbiaceae, and Molluginaceae, respectively. The families that correlated to LST show the bearing of these families to high temperatures. Legally, the

http://www.aloki.hu ● ISSN 1589 1623 (Print) ● ISSN 1785 0037 (Online)
DOI: http://dx.doi.org/10.15666/aeer/2203_25672587

designation of a wildlife-protected area is insufficient to stop overdevelopment. In order to protect the site, it should be given protected area status, which would encourage the increase in vegetation cover in such locations. The results of this present study will also help decision-makers take measures or decisions for future development.

Conflict of interests. The author declares no competing interests.

REFERENCES

[1] Abd El-Hamid, H. T. (2020): Geospatial analyses for assessing the driving forces of land use/land cover dynamics around the Nile Delta branches, Egypt. – J Indian Soc Remote Sens 48: 1661-1674.

[2] Barsi, J. A., Schott, J. R., Hook, S. J., Raqueno, N. G., Markham, B. L., Radocinski, R. G. (2014): Landsat-8 thermal infrared sensor (TIRS) vicarious radiometric calibration. – Remote Sensing 6(11): 11607-11626.

[3] Bonn, F. J., O'Neill, N. T. (1993): Thermal infrared remote sensing of soils: evolution, trends and perspectives. – Remote Sens. Rev. 7: 281-302.

[4] Chandra, N., Singh, G., Rai, I. D., Mishra, A. P., Kazmi, M. Y., Pandey, A., Abdo, H. G. (2023): Predicting distribution and range dynamics of three threatened Cypripedium Species under climate change scenario in Western Himalaya. – Forests 14(3): 633. https://doi.org/10.3390/f14030633.

[5] Chaudhary, S. A. (1989): Grasses of Saudi Arabia. – National Herbarium, National Agriculture and Water Research Center, Ministry of Agriculture and Water, Riyadh.

[6] Chen, X., Zhao, H., Li, P., Yin, Z. (2006): Remote sensing image-based analysis of the relationship between urban heat island and land use/cover changes. – Remote Sensing of Environment 104(2): 133-146. DOI: 10.1016/j.rse.2005.11.016.

[7] Choe, Y.-J., Yom, J.-H. (2020): Improving accuracy of land surface temperature prediction model based on deep-learning. – Spat. Inf. Res. 28: 377-382.

[8] Collentette, S. (1999): Wildflowers of Saudi Arabia. – National Commission for Wildlife Conservation and Development, Riyadh.

[9] Elaidarous, A. A., Osman, H. E., Galal, T. M., El-Morsy, M. H. (2022): Vegetation–environment relationship and floristic diversity of Wadi Al-Sharaea, Makkah Province, Saudi Arabia. – Rend. Fis. Acc. Lincei 33: 169-184. https://doi.org/10.1007/s12210-022-01047-y.

[10] Feddema, J. J., Oleson, K. W., Bonan, G. B., Mearns, L. O., Buja, L. E., Meehl, G. A., Washington, W. M. (2005): The importance of land-cover change in simulating future climates. – Science 1674-1678.

[11] Folland, C. K., Karl, T. R., Vinnikov, K. Y. A. (1990): Observed Climate Variations and Change. – In: Houghton, J. T., Jenkins, G. J., Ephraums, J. J. (eds.) Climate Change: The IPCC Scientific Assessment. University Press, Cambridge, pp. 195-238.

[12] Guha, S., Govil, H., Dey, A., Gill, N. (2018): Analytical study of land surface temperature with NDVI and NDBI using Landsat 8 OLI and TIRS data in Florence and Naples City, Italy. – Europ. J. Remot. Sens. 51(1): 667-678. https://doi.org/10.1080/22797254.2018.1474494.

[13] Hussain, S., Raza, A., Abdo, H. G. et al (2023): Relation of land surface temperature with different vegetation indices using multi-temporal remote sensing data in Sahiwal region, Pakistan. – Geosci. Lett. 10: 33. https://doi.org/10.1186/s40562-023-00287-6.

[14] Ibrahim, F., Rasul, G. (2017): Urban land use land cover changes and their effect on land surface temperature: case study using dohuk city in the Kurdistan Region of Iraq. – Climate 5(1): 13. https://doi.org/10.3390/cli5010013.

[15] Islam, M. S., Fahad, S., Hossain, A., Chowdhury, M. K., Iqbal, M. A., Dubey, A., Sabagh, A. E. (2021): Legumes under Drought Stress: Plant Responses, Adaptive Mechanisms, and Management Strategies in Relation to Nitrogen Fixation. – In: Fahad, S., Sönmez, O., Saud, S., Wang, D., Wu, C., Adnan, M., Arif, M. (eds.) Engineering Tolerance in Crop Plants Against Abiotic Stress. CRC Press, Boca Raton.

[16] Joshi, R. C., Ryu, D., Sheridan, G. J., Lane, P. N. J. (2020): A new remote sensing-based vegetation water stress index: temperature vegetation water stress index (TVWSI). – EGU General Assembly, Online, 4-8 May 2020. EGU2020-12308. https://doi.org/10.5194/egusphereegu2020-12308.

[17] Kant, Y., Bharath, B. D., Mallick, J., Atzberger, C., Kerle, N. (2009): Satellite-based analysis of the role of land use/land cover and vegetation density on surface temperature regime of Delhi, India. – J. Indian Soc. Remote Sens. 37: 201-214.

[18] Ludwig, J. A., Reynolds, J. F. (1988): Statistical Ecology: A Primer on Methods and Computing. – Wiley, New York.

[19] Malik, M. S., Shukla, J. P., Mishra, S. (2019): Relationship of LST-NDBI and NDVI using Landsat 8 data in Kandaihimmat Watershed, Hoshangabad, India. – Indian J. Geo-Marine Sci. 48(1): 25-31.

[20] Maskooni, E. K., Hashemi, H., Berndtsson, R., Arasteh, P. D., Kazemi, M. (2021): Impact of spatio temporal land-use and land cover changes on surface urban heat islands in a semi-arid region using Landsat data. – International Journal of Digital Earth 14(2): 250-270. DOI: 10.1080/17538947.2020.1813210.

[21] Migahid, A. M. (1996): Flora of Saudi Arabia. 4th Ed. – King Saud University Press, Riyadh.

[22] Mondino, E. B., Lessio, A., Gomarasca, M. A. (2016): A fast operative method for NDVI uncertainty estimation and its role in vegetation analysis. – European Journal of Remote Sensing 49(1): 137-156. DOI: 10.5721/EuJRS20164908.

[23] Morrison, J. M., Goldhaber, M. B., Ellefsen, K. J. Mills, C. T. (2011): Cluster analysis of a regional scale soil geochemical dataset in northern California. – Applied Geochemistry 26: 105-107.

[24] Mueller-Dombois, D., Ellenberg, H. (1974): Aims and Methods of Vegetation Ecology. – John Wiley and Sons, New York.

[25] Müller, B., Bernhardt, M., Jackisch, C., Schulz, K. (2016): Estimating spatially distributed soil texture using time series of thermal remote sensing: a case study in central Europe. – Hydrol. Earth Syst. Sci. 20: 3765-3775.

[26] Osińka-Skotak, K. (2007): Studies of soil temperature on the basis of satellite data. – Int. Agrophys. 21.

[27] Ranagalage, M., Estoque, R. C., Zhang, X., Murayama, Y. (2018): Spatial changes of urban heat island formation in the Colombo District, Sri Lanka: implications for sustainability planning. – Sustainability 10(5): 1367. DOI: 10.3390/su10051367.

[28] Rani, M., Kumar, P., Pandey, P. C., Srivastava, P. K., Chaudhary, B. S., Tomar, V., Mandal, V. P. (2018): Multi-temporal NDVI and surface temperature analysis for Urban Heat Island inbuilt surrounding of sub-humid region: a case study of two geographical regions. – Remote Sens App Soc Environ 10: 163-172. https://doi.org/10.1016/j.rsase.2018.03.007.

[29] Rimal, B., Zhang, L., Keshtkar, H., Wang, N., Lin, Y. I. (2017): Monitoring and modeling of spatiotemporal urban expansion and land-use/land-cover change using integrated Markov chain cellular automata model. – ISPRS Int. J. Geo Inf. 6(9): 288.

[30] Roy, S., Pandit, S., Eva, E. A. S., Bagmar, H., Papia, M., Banik, L., Dube, T., Rahman, F., Razi, M. A. (2020): Examining the nexus between land surface temperature and urban growth in Chattogram Metropolitan area of Bangladesh using long term Landsat series data. – Urban Climate 32. 100593. DOI: 10.1016/j.uclim.2020.100593.

http://www.aloki.hu ● ISSN 1589 1623 (Print) ● ISSN 1785 0037 (Online)
DOI: http://dx.doi.org/10.15666/aeer/2203_25672587

[31] Sobrino, J. A., Caselles, V., Becker, F. (1990): Significance of the remotely sensed thermal infrared measurements obtained over a citrus orchard. – ISPRS Photogramm Eng Remote Sensing 44: 343-354.
[32] Tadini, A. M., Xavier, A. A., Milori, D. M., Oliveira, P. P., Pezzopane, J. R., Bernardi, A. C., Martin-Neto, L. (2021): Evaluation of soil organic matter from integrated production systems using laser-induced fluorescence spectroscopy. – Soil Tillage Res. 211: 105001.
[33] Wang, D. C., Zhang, G. L., Pan, X. Z., Zhao, Y. G., Zhao, M. S., Wang, G. F. (2012): Mapping soil texture of a plain area using fuzzy-c-means clustering method based on land surface diurnal temperature difference. – Pedosphere 22: 394-403.
[34] Wang, D. C., Zhang, G. L., Zhao, M. S., Pan, X. Z., Zhao, Y. G., Li, D. C., Macmillan, B. (2015): Retrieval and mapping of soil texture based on land surface diurnal temperature range data from MODIS. – PLoS One 10.
[35] Weng, Q., Lu, D. (2008): A sub-pixel analysis of urbanization effect on land surface temperature and its interplay with impervious surface and vegetation coverage in Indianapolis, United States. – International Journal of Applied Earth Observation and Geoinformation 10(1): 68-83. DOI: http://dx.doi.org/10.1016/j.jag.2007.05.002.
[36] Weng, Q., Lu, D., Schubring, J. (2004): Estimation of land surface temperature–vegetation abundance relationship for urban heat island studies. – Remote Sensing of Environment 89(4): 467-483. http://dx.doi.org/10.1016/j.rse.2003.11.005.
[37] Xu, C., Zhang, Y. (2017): Impacts of urban surface characteristics on spatiotemporal pattern of land surface temperature in Kunming of China. – Sustainable Cities and Society 32(July): 87-99. DOI: 10.1016/j.scs. 2017.03.013.
[38] Zhang, X., Estoque, R. C., Murayama, Y., Ranagalage, M. (2021): Capturing urban heat island formation in a subtropical city of China based on Landsat images: implications for sustainable urban development. – Environ. Monit. Assess. 193: 1-13.
[39] Zhao, H. M., Chen, X. L. (2005): Use of normalized difference bareness index in quickly mapping bare areas from TM/ETM+. – Proceedings of 2005 IEEE International Geoscience and Remote Sensing Symposium, Seoul, Korea 3: 25-29.
[40] Zhao, M. S., Rossiter, D. G., Li, D. C., Zhao, Y. G., Liu, F., Zhang, G. L. (2014): Mapping soil organic matter in low-relief areas based on land surface diurnal temperature difference and a vegetation index. – Ecol. Indic. 39: 120-133.

APPENDIX

Table A1. *Measurements (density, coverage, frequency, importance value) of Wadi Al-Sharaea, Makkah Province, Saudi Arabia*

Scientific name	PC	RC	D	RD	F	RF	IV
Blepharis ciliaris	0.01	0.06	0.008	0.59	3.92	0.55	1.20
Blepharis edulis	0.008	0.04	0.002	0.11	2.94	0.41	0.57
Aizoon canariense	0.02	0.09	0.005	0.37	5.88	0.83	1.29
Sesuvium verrucosum	0.002	0.010	0.0004	0.03	0.98	0.14	0.18
Trianthema portulacastrum	0.0008	0.004	0.001	0.08	1.96	0.28	0.37
Trianthema triquetra	0.0002	0.001	0.0004	0.03	0.98	0.14	0.17
Zaleya pentandra	0.06	0.31	0.004	0.25	3.92	0.55	1.12
Aerva javanica	0.07	0.37	0.02	1.38	11.76	1.66	3.42
Amaranthus graecizans	0.04	0.20	0.009	0.65	14.71	2.07	2.92
Amaranthus viridis	0.04	0.22	0.003	0.20	3.92	0.55	0.97
Digera muricata	0.02	0.10	0.001	0.08	2.94	0.41	0.60
Kaviria lachnantha	0.00002	0.0001	0.0004	0.03	0.98	0.14	0.17
Calotropis procera	0.07	0.34	0.002	0.17	5.88	0.83	1.34
Cynanchum radians	0.0002	0.0010	0.0008	0.06	0.98	0.14	0.20

http://www.aloki.hu ● ISSN 1589 1623 (Print) ● ISSN 1785 0037 (Online)
DOI: http://dx.doi.org/10.15666/aeer/2203_25672587

Scientific name	PC	RC	D	RD	F	RF	IV
Leptadenia pyrotechnica	0.31	1.57	0.004	0.28	3.92	0.55	2.40
Rhazya stricta	3.59	18.45	0.03	1.81	27.45	3.87	24.13
Lemna gibba	0.01	0.04	0.02	1.41	0.98	0.14	1.59
Asphodelus tenuifolius	0.0002	0.0010	0.0004	0.03	0.98	0.14	0.17
Anvillea garcinii	0.0001	0.0007	0.0004	0.03	0.98	0.14	0.17
Eclipta prostrata	0.006	0.03	0.0004	0.03	0.98	0.14	0.20
Flaveria trinervia	0.0003	0.001	0.0004	0.03	0.98	0.14	0.17
Launaea intybacea	0.006	0.03	0.0008	0.06	1.96	0.28	0.36
Picris cyanocarpa	0.004	0.02	0.0004	0.03	0.98	0.14	0.18
Pulicaria schimperi	0.004	0.02	0.0020	0.14	2.94	0.41	0.58
Sonchus oleraceus	0.01	0.06	0.003	0.20	3.92	0.55	0.81
Euploca strigosa	0.0002	0.001	0.0004	0.03	0.98	0.14	0.17
Heliotropium aegyptiacum	0.0010	0.005	0.0004	0.03	0.98	0.14	0.17
Heliotropium arbainense	0.0020	0.0101	0.0004	0.03	0.98	0.14	0.18
Heliotropium curassavicum	0.005	0.03	0.0008	0.06	0.98	0.14	0.22
Heliotropium lasiocarpum	0.0009	0.004	0.001	0.08	0.98	0.14	0.23
Heliotropium longiflorum	0.005	0.03	0.002	0.11	2.94	0.41	0.55
Heliotropium pterocarpum	0.12	0.62	0.02	1.69	23.53	3.32	5.64
Trichodesma africanum	0.008	0.04	0.0008	0.06	0.98	0.14	0.23
Farsetia aegyptia	0.08	0.41	0.005	0.34	3.92	0.55	1.30
Morettia parviflora	0.26	1.34	0.02	1.50	5.88	0.83	3.67
Sisymbrium irio	0.002	0.0081	0.0004	0.03	0.98	0.14	0.17
Maerua crassifolia	0.16	0.81	0.0008	0.06	1.96	0.28	1.14
Polycarpaea repens	0.09	0.46	0.10	7.09	39.22	5.53	13.08
Polycarpaea robbairea	0.14	0.70	0.03	1.86	11.76	1.66	4.22
Cleome chrysantha	0.00005	0.0002	0.0004	0.03	0.98	0.14	0.17
Cleome pallida	0.22	1.13	0.0718	5.17	33.33	4.70	11.01
Cleome scaposa	0.003	0.02	0.002	0.17	3.92	0.55	0.74
Convolvulus cephalopodus subsp. bushiricus	0.005	0.03	0.0004	0.03	0.98	0.14	0.19
Citrullus colocynthis	0.92	4.72	0.03	1.84	33.33	4.70	11.26
Citrullus lanatus	0.003	0.01	0.0004	0.03	0.98	0.14	0.18
Coccinia grandis	0.003	0.02	0.0004	0.03	0.98	0.14	0.18
Euphorbia arabica	0.001	0.008	0.0004	0.03	0.98	0.14	0.17
Euphorbia granulata	0.02	0.13	0.02	1.10	15.69	2.21	3.44
Astragalus vogelii	0.001	0.006	0.0008	0.06	0.98	0.14	0.20
Crotalaria microphylla	0.03	0.17	0.02	1.33	17.65	2.49	3.99
Indigofera hochstetteri	0.008	0.04	0.0020	0.14	1.96	0.28	0.46
Indigofera sessiliflora	0.003	0.01	0.001	0.08	1.96	0.28	0.38
Indigofera spinosa	0.01	0.06	0.002	0.11	2.94	0.41	0.58
Prosopis juliflora	0.50	2.59	0.008	0.59	9.80	1.38	4.56
Senna alexandrina	0.27	1.41	0.001	0.08	2.94	0.41	1.91
Senna italica	0.42	2.14	0.03	2.03	23.53	3.32	7.50
Tephrosia nubica	0.02	0.12	0.0008	0.06	1.96	0.28	0.46
Vachellia flava	0.91	4.68	0.007	0.48	10.78	1.52	6.69
Vachellia seyal	0.002	0.01	0.0004	0.03	0.98	0.14	0.18
Vachellia tortilis	0.02	0.08	0.0004	0.03	0.98	0.14	0.25
Vachellia tortilis subsp. raddiana	1.59	8.15	0.010	0.71	10.78	1.52	10.38
Gisekia pharnaceoides	0.13	0.65	0.03	2.40	28.43	4.01	7.06
Ocimum forskoelei	0.002	0.01	0.0004	0.03	0.98	0.14	0.18
Limeum obovatum	0.003	0.01	0.0020	0.14	1.96	0.28	0.43
Abutilon pannosum	0.002	0.009	0.0004	0.03	0.98	0.14	0.18
Corchorus depressus	0.0004	0.002	0.0004	0.03	0.98	0.14	0.17
Malva parviflora	0.0008	0.004	0.0004	0.03	0.98	0.14	0.17
Glinus lotoides	0.94	4.84	0.07	5.25	7.84	1.11	11.20

Scientific name	PC	RC	D	RD	F	RF	IV
Hypertelis cerviana	0.06	0.30	0.07	4.97	22.55	3.18	8.45
Neurada procumbens	0.004	0.02	0.004	0.28	3.92	0.55	0.85
Boerhavia diffusa	0.09	0.44	0.01	0.76	12.75	1.80	3.00
Boerhavia repens	0.01	0.05	0.0008	0.06	0.98	0.14	0.25
Commicarpus helenae	0.01	0.05	0.001	0.08	1.96	0.28	0.41
Lindenbergia indica	0.08	0.39	0.003	0.20	0.98	0.14	0.72
Aristida abnormis	0.18	0.91	0.04	2.94	14.71	2.07	5.93
Aristida funiculata	1.34	6.89	0.08	6.10	5.88	0.83	13.82
Cenchrus americanus	0.01	0.06	0.0004	0.03	0.98	0.14	0.23
Cenchrus biflorus	0.005	0.02	0.005	0.34	3.92	0.55	0.92
Cenchrus ciliaris	0.02	0.12	0.001	0.08	0.98	0.14	0.34
Cenchrus divisus	0.32	1.67	0.04	2.54	18.63	2.63	6.84
Cenchrus pennisetiformis	0.07	0.35	0.003	0.23	5.88	0.83	1.41
Cenchrus setiger	0.18	0.91	0.001	0.08	0.98	0.14	1.13
Centropodia forskalii	0.01	0.06	0.005	0.40	6.86	0.97	1.42
Chloris barbata	0.006	0.03	0.0004	0.03	0.98	0.14	0.20
Cynodon dactylon	0.05	0.26	0.004	0.31	2.94	0.41	0.98
Digitaria nodosa	0.01	0.08	0.0004	0.03	0.98	0.14	0.24
Digitaria sanguinalis	0.02	0.12	0.001	0.08	1.96	0.28	0.48
Echinochloa colonum	0.07	0.34	0.005	0.37	6.86	0.97	1.68
Eleusine africana	0.01	0.03	0.0004	0.03	0.98	0.14	0.19
Eragrostis cilianensis	0.01	0.06	0.005	0.40	6.86	0.97	1.43
Eragrostis ciliaris	0.02	0.13	0.005	0.40	3.92	0.55	1.08
Eragrostis curvula	0.33	1.70	0.02	1.10	1.96	0.28	3.08
Panicum turgidum	0.69	3.53	0.02	1.19	18.63	2.63	7.34
Stipagrostis hirtigluma	0.010	0.05	0.002	0.11	2.94	0.41	0.58
Stipagrostis plumosa	2.84	14.59	0.16	11.61	22.55	3.18	29.35
Rumex vesicarius	0.001	0.0060	0.0004	0.03	0.98	0.14	0.17
Portulaca oleracea	0.008	0.04	0.004	0.25	6.86	0.97	1.26
Kohautia caespitosa	0.02	0.12	0.004	0.28	8.82	1.24	1.65
Haplophyllum tuberculatum	0.007	0.03	0.004	0.31	6.86	0.97	1.31
Datura innoxia	0.08	0.43	0.002	0.14	3.92	0.55	1.13
Solanum nigrum	0.005	0.02	0.0004	0.03	0.98	0.14	0.19
Solanum villosum	0.008	0.04	0.0004	0.03	0.98	0.14	0.21
Tamarix aphylla	0.01	0.06	0.0008	0.06	0.98	0.14	0.26
Forsskaolea tenacissima	0.0004	0.002	0.002	0.11	1.96	0.28	0.39
Tribulus bimucronatus	0.01	0.07	0.0008	0.06	0.98	0.14	0.26
Tribulus macropterus	0.25	1.30	0.08	5.8	26.47	3.72	10.83
Tribulus pentandrus	1.33	6.81	0.19	13.53	21.57	3.04	23.40
Tribulus terrestris	0.0020	0.01	0.0004	0.03	0.98	0.14	0.18
Zygophyllum indicum	0.02	0.09	0.004	0.28	7.84	1.11	1.48
Zygophyllum simplex	0.06	0.32	0.02	1.19	20.59	2.90	4.41
Total	**19.46**	**100.00**	**1.41**	**100**	**708.74**	**100**	**300.00**

D: density, RD: relative density, PC: plant cover, RC: relative cover, F: frequency, RF: relative frequency, IV: Importance value

Table A2. *Floristic features of the recorded species in Wadi Al-Sharaea during autumn and spring from 2018 to 2021*

Family	Scientific name	Vegetation type	Palatability	P. P	Life form	Floristic categories	A
Acanthaceae	*Blepharis ciliaris* (L.)	Per.	P	C4	CH	IT+SA+SZ	co
	Blepharis edulis (Forssk.) Pers.	Ann.	P	C4	CH	SA+SZ	co
Aizoaceae	*Aizoon canariense* L.	Ann.	P	C3	HE	IT+ME+SA+TR	co
	Sesuvium verrucosum Raf.	Ann.	P	C3	HE	SA+SZ	cc

http://www.aloki.hu ● ISSN 1589 1623 (Print) ● ISSN 1785 0037 (Online)
DOI: http://dx.doi.org/10.15666/aeer/2203_25672587

Family	Scientific name	Vegetation type	Palatability	P. P	Life form	Floristic categories	A
	Trianthema portulacastrum L.	Ann.	P	C4	TH	SZ+TR	ra
	Trianthema triquetra Willd	Ann.	P	C4	TH	IT+SZ+TR	ra
	Zaleya pentandra (L.) C. Jeffrey.	Per.	P	C4	HE	SZ	ra
Amaranthaceae	*Aerva javanica* (Burm.f.) Juss.	Per.	P	C4	CH	SA+SZ+TR	co
	Amaranthus graecizans L.	Ann.	P	C4	TH	PAL (Weed)	co
	Amaranthus viridis L.	Ann.	P	C4	TH	COSM	co
	Digera muricata (L.) Mart.	Ann.	P	C3	TH	PAL	ra
	Kaviria lachnantha (Botsch.) Akhani (*Salsola lachnantha* (Botsch.)	Per.	P	C3	CH	SA	cc
Apocynaceae	*Calotropis procera* (Aiton) W.T.Aiton	Per.	P	C3	PH	SA+SZ	co
	Odontanthera radians (Forssk.)	Per.	Up	C3	HE	SZ	ra
	Leptadenia pyrotechnica (Forssk.)Decne.	Per.	P	C4	CH	SA+SZ	co
	Rhazya stricta Decne.	Per.	UP	C3	CH	SA+SZ	cc
Araceae	*Lemna gibba* L.	Per.	P	C3	HY	COSM	co
Asphodelaceae	*Asphodelus tenuifolius* Cav.	Ann.	P	C3	GH	IT+ME+SA	co
Asteraceae	*Anvillea garcinii* (Burm.f.) DC.	Ann.	P	C3	CH	IT+SA+SZ	co
	Eclipta prostrata (L.) L.	Ann.	P	C3	TH	SA+SZ	ra
	Flaveria trinervia (Spreng.) C.Mohr	Ann.	P	C4	CH	SZ+TR	cc
	Launaea intybacea (Jacq.)Beauverd.	Ann.	P	C3	TH	IT+SA+SZ+PAN	ra
	Picris cyanocarpa Boiss.	Ann.	P	C3	TH	SZ	ra
	Pulicaria schimperi DC.	Per.	P	C3	CH	SA+SZ	ra
	Sonchus oleraceus L.	Ann.	P	C3	TH	ES+IT+ME	ra
Boraginaceae	*Euploca strigosa* (Willd.) Diane & Hilger	Ann.	P	C4	TH	SA+SZ	ra
	Heliotropium egyptiacum Lehm.	Ann.	Up	C3	CH	SA+SZ	vr
	Heliotropium arbainense Fresen.	Per.	Up	C3	CH	SA+SZ	co
	Heliotropium curassavicum L.	Per.	Up	C4	CH	PAN	co
	Heliotropium lasiocarpum Fisch. & C.A.Mey.	Per.	Up	C3	CH	SA+SZ	co
	Heliotropium longiflorum (A.DC.) Jaub. & Spach	Per.	Up	C3	CH	SA+SZ	ra
	Heliotropium pterocarpum (DC.) Hochst. & Steud. ex Bunge	Ann.	Up	C3	CH	SA+SZ	ra
	Trichodesma africanum (L.) Sm.	Ann.	Up	C3	TH	SA+SZ	ra
Brassicaceae	Farsetia aegyptia Turra.	Per.	Up	C3	CH	SS+SZ	co
	Morettia parviflora Boiss.	Per.	P	C3	TH	SZ	co
	Sisymbrium irio L.	Ann.	P	C3	TH	IT+ME+SA+SZ	ra
Capparaceae	*Maerua crassifolia* Forssk.	Per.	P	C3	PH	IT+ME+SA+SZ	co
Caryophyllaceae	*Polycarpaea repens* (Forssk.) Asch. & Schweinf.	Per.	P	C3	CH	SA+SZ	co
	Polycarpaea robbairea (Kuntze) Greuter & Burdet	Per.	P	C3	TH	ME	ra
Cleomaceae	*Cleome chrysantha* Decne.	Per.	Up	C3	CH	SA	ra
	Dipterygium glaucum Decne (Cleome pallida Kotschy.)	Per.	P	C3	CH	SZ	co
	Gilgella scaposa (DC.) Roalson & J.C.Hall (Cleome scaposa DC.)	Ann.	P	C3	TH	SA+SZ	ra
Convolvulaceae	*Convolvulus cephalopodus* subsp. bushiricus (Bornm.)	Per.	Up	C3	CH	SA	ra
Cucurbitaceae	*Citrullus colocynthis*(L.) Schrad.	Per.	P	C3	HE	ME+SS+IT+SZ	co
	Citrullus lanatus (Thunb.) Matsum. & Nakai.	Ann.	P	C3	HE	COSM	co
	Coccinia grandis (L.) Voigt.	Per.	Up	C3	HE	PAL	vr
Euphorbiaceae	*Euphorbia arabica* Hochst. & Steud.	Ann.	P	C3	HE	ME+SA+SZ	ra

http://www.aloki.hu ● ISSN 1589 1623 (Print) ● ISSN 1785 0037 (Online)
DOI: http://dx.doi.org/10.15666/aeer/2203_25672587

Family	Scientific name	Vegetation type	Palatability	P. P	Life form	Floristic categories	A
	ex T.Anderson						
	Euphorbia granulata Forssk	Ann.	P	C3	TH	SA+SZ	co
Fabaceae	*Astragalus vogelii* (Webb) Bornm.	Ann.	P	C3	CH	ME+SA+SZ+TR	ra
	Crotalaria microphylla Vahl.	Ann.	P	C3	TH	SA+SZ	vr
	Indigofera hochstetteri Baker.	Ann.	P	C3	TH	SS+SZ	co
	Indigofera sessiliflora DC.	Ann.	P	C3	TH	IT+SA+TR	vr
	Indigofera spinosa Forssk.	Per.	P	C3	CH	SA+SZ	co
	Prosopis juliflora (Sw.) DC.	Per.	P	C3	PH	SA	co
	Senna alexandrina Mill.	Per.	Up	C3	CH	SA+SZ	ra
	Senna italica Mill.	Per.	Up	C3	CH	SA+SZ	co
	Tephrosia nubica (Boiss.) Baker.	Pre.	Up	C3	CH	SA	ra
	Vachellia flava (Forssk.) Kyal. & Boatwr. (*Acacia ehrenbergiana* Hayne.)	Per.	P	C3	PH	SA+SZ	co
	Vachellia seyal (Delile) P.J.H.Hurter. (Acacia seyal Delile.)	Per.	P	C3	PH	SA+SZ	co
	Vachellia tortilis (Forssk.) Galasso & Banfi. (*Acacia tortilis* (Forssk.) Hayne.)	Per.	P	C3	PH	SZ	co
	Vachellia tortilis subsp. raddiana (Savi) Kyal. & Boatwr. (Acacia raddiana (Savi))	Per.	P	C3	PH	SZ	co
Gisekiaceae	*Gisekia pharnaceoides* L.	Ann.	P	C4	TH	SA+TR	co
Lamiaceae	*Ocimum forskoelei* Benth.	Per.	Up	C3	HE	SA	ra
Limeaceae	*Limeum obovatum* Vicary.	Per.	P	C3	HE	IT+SS+SZ	ra
Malvaceae	*Abutilon pannosum* (G.Forst.) Schltdl.	Per.	P	C3	CH	IT+SA+SZ	co
	Corchorus depressus (L.) Peterm.	Per.	P	C3	TH	ME+SA	vr
	Malva parviflora L.	Ann.	P	C3	TH	IT+ME	co
Molluginaceae	*Glinus lotoides* L.	Ann.	P	C3	TH	IT+ME+TR	ra
	Hypertelis cerviana (L.) Thulin. (Mollugo cerviana (L.) Ser.)	Ann.	P	C3	TH	SA+SS+SZ+TR	co
Neuradacaeae	*Neurada procumbens* L.	Ann.	P	C3	TH	SA+SZ	ra
Nyctaginaceae	*Boerhavia diffusa* L.	Ann.	P	C4	CH	SA+TR	ra
	Boerhavia repens L.	Ann	P	C4	CH	SA+SZ+PAN	ra
	Commicarpus helenae (Roem. & Schultes) Meikle	Per.	Up	C3	CH	IT+SA	ra
Orobanchaceae	Lindenbergia indica (L.) Vatke	Per.	Up	C3	TH	PAL	ra
Poaceae	Aristida abnormis Chiov.	Ann.	P	C4	TH	PAL	ra
	Aristida funiculata Trin. &	Ann.	P	C4	TH	IT+SA	ra
	Cenchrus americanus (L.) Morrone	Per.	P	C4	GH	PAL	cc
	Cenchrus biflorus Roxb.	Ann	P	C3	GH	SS+SZ	co
	Cenchrus ciliaris L.	Per.	P	C4	GH	COSM	co
	Cenchrus divisus (J.F.Gmel.) Verloove, Govaerts & Buttler. (Pennisetum divisum)	Per.	P	C3	GH	SA+SS+SZ	co
	Cenchrus pennisetiformis Steud.	Ann.	P	C3	TH	IT+SA	ra
	Cenchrus setiger Vahl	Per.	P	C4	TH	PAL	co
	Centropodia forskalii (Vahl) Cope	Per.	P	C3	GH	IT+SA	ra
	Chloris barbata Sw.	Ann.	P	C4	HE	SZ	ra
	Cynodon dactylon (L.) Pers.	Per.	P	C4	GH	COSM	co
	Digitaria nodosa Parl.	Ann.	P	C4	TH	COSM	co
	Digitaria sanguinalis (L.) Scop.	Ann	P	C4	TH	PAL	co
	Echinochloa colonum (L.) Link	Ann.	P	C4	TH	COSM	co
	Eleusine africana Kenn.-O'Byrne	Ann.	P	C4	TH	PAL	vr

http://www.aloki.hu ● ISSN 1589 1623 (Print) ● ISSN 1785 0037 (Online)
DOI: http://dx.doi.org/10.15666/aeer/2203_25672587

Family	Scientific name	Vegetation type	Palatability	P. P	Life form	Floristic categories	A
	Eragrostis cilianensis (All.) Vignolo ex Janch.	Ann.	P	C4	TH	PAL	vr
	Eragrostis ciliaris (L.) R.Br.	Ann.	P	C3	TH	SZ+TR	co
	Eragrostis curvula (Schrad.)	Per.	P	C4	TH	IT+SS+TR	vr
	Panicum turgidum Forssk	Per.	P	C4	GH	IT+ME+SZ	co
	Stipagrostis hirtigluma (Steud. ex Trin. & Rupr.) De Winter	Ann.	P	C4	HE	SA+SZ	ra
	Stipagrostis plumosa (L.) Munro	Per.	P	C4	GH	COSM	co
Polygonaceae	*Rumex vesicarius* L.	Ann	P	C3	TH	ME+SA+SZ	co
Portulacaceae	*Portulaca oleracea* L.	Ann.	P	C4	TH	COSM (Weed)	co
Rubiaceae	*Kohautia caespitosa* Schnizl.	Ann.	P	C3	CH	IT+SA	c
Rutaceae	*Haplophyllum tuberculatum* (Forssk.) A. Juss.	Per.	P	C3	CH	IT+SS	co
Solanaceae	*Datura innoxia* Mill.	Per.	Up	C3	CH	NEO+PAL	ra
	Solanum nigrum L.	Ann.	P	C3	CH	COSM (Weed)	co
	Solanum villosum Mill.	Ann.	P	C3	CH	ES+IT+ME	co
Tamaricaceae	*Tamarix aphylla* (L.) H.Karst.	Per.	P	C3	PH	IT+SA+SZ	co
Urticaceae	*Forsskaolea tenacissima* L.	Ann.	P	C3	CH	SA+SZ	co
Zygophyllaceae	*Tribulus bimucronatus* Viv.	Ann.	p	C3	HE	SA+SZ	co
	Tribulus macropterus Boiss.	Ann.	P	C3	HE	SZ	co
	Tribulus pentandrus Forssk.	Ann.	p	C4	TH	SA+SZ	co
	Tribulus terrestris L.	Ann.	P	C4	TH	ES+IT+SA+SZ	cc
	Zygophyllum indicum (Burm.f.) Christenh. & Byng.	Per.	P	C3	CH	IT+SA	co
	Zygophyllum simplex L.	Ann.	P	C4	TH	SA+SZ	co

P. P: photosynthetic pathway, *Ann* Annual, *Per* Perennial, palatability, *P* Palatable, *Up* Unpalatable, *A* abundance, *co* common, *vc* very common, *ra* rare, *rr* very rare, Life forms: *TH* therophytes, *CH* chamaephytes, *PH* phanerophytes, *HE* hemicryptophytes, *GH* geophytes, *HY* hydrophytes, Floristic categories (Chorotypes): *COSM* Cosmopolitan, *IT* Irano-Turanian, *ME* Mediterranean, *PAN* pantropical, *PAL* palaeotropical, *NEO* neotropical, *SA* Saharo-Arabian, *SS* Saharo-Sindian, *SZ* Sudano-Zambesian, *TR* tropical